Supporting Information

Efficient CO_2 Capture from Ambient Air with Amine-Functionalized Mg–Al Mixed Metal Oxides

Xuancan Zhu,[a] Tianshu Ge,*[a] Fan Yang,[a] Meng Lyu,[b] Chunping Chen,[b] Dermot O'Hare,[b] and Ruzhu Wang*[a]

a Research Center of Solar Power & Refrigeration, School of Mechanical Engineering, Shanghai Jiao Tong University, 800 Dongchuan Road, Shanghai, 200240, China. E-mail: baby_wo@sjtu.edu.cn; rzwang@sjtu.edu.cn
b Chemistry Research Laboratory, Department of Chemistry, University of Oxford, 12 Mansfield Road, Oxford, OX1 3TA, UK

Table S1. ICP-OES results of Mg and Al contents in the prepared MMO precursors.

	$Mg_{0.55}Al\text{-}CO_3$		$Mg_2Al\text{-}CO_3$		$Mg_3Al\text{-}CO_3$	
	Mg2852	Al3961	Mg2852	Al3961	Mg2852	Al3961
Units	wt.%	wt.%	wt.%	wt.%	wt.%	wt.%
Avg	9.732	20.13	18.42	10.96	22.08	8.567
Stddev	0.019	0.05	0.08	0.08	0.14	0.062
% RSD	0.1908	0.2547	0.4509	0.6931	0.6349	0.7202
Rep #1	9.726	20.12	18.50	11.03	22.29	8.658
Rep #2	9.711	20.08	18.47	11.03	21.96	8.526
Rep #3	9.737	20.14	18.32	10.88	22.05	8.552
Rep #4	9.755	20.20	18.38	10.91	22.03	8.530
x (set)	0.55		2		3	
x (exp)	0.537		1.866		2.861	

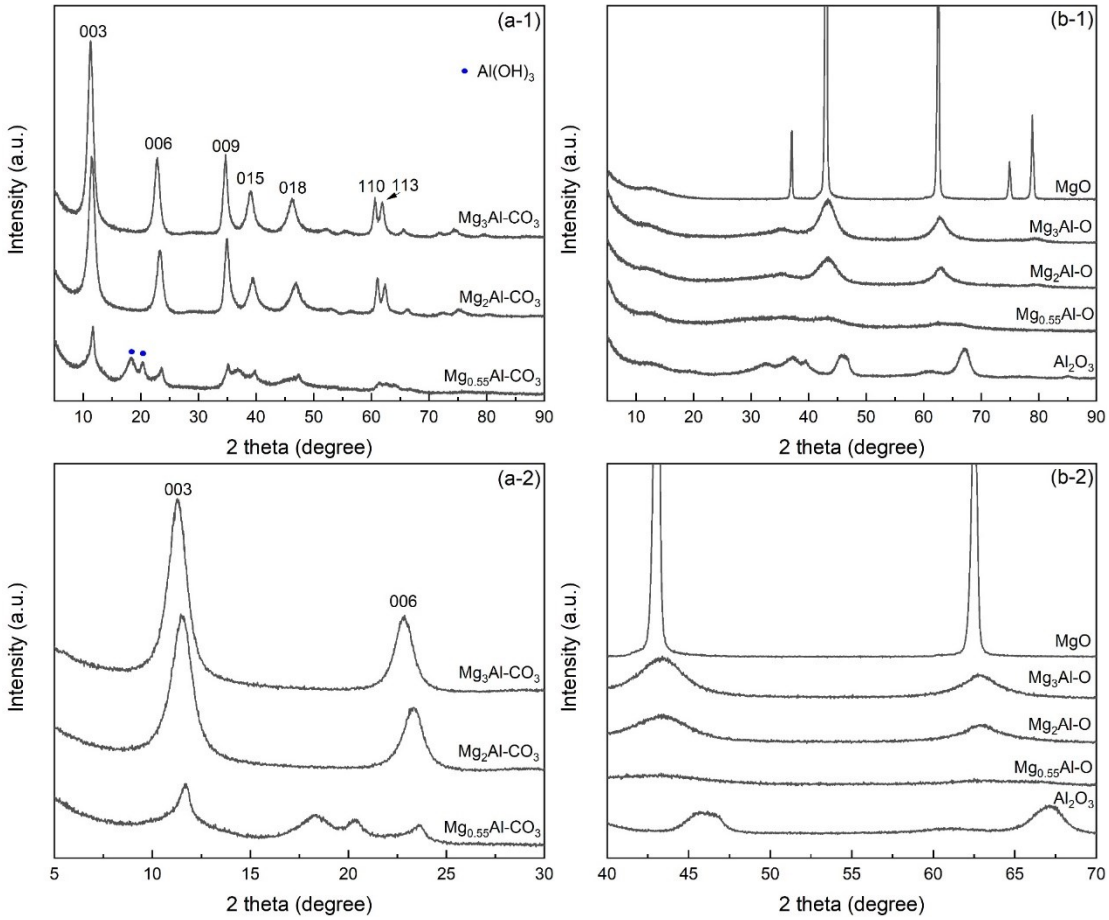

Figure S1. XRD patterns of (a) MMO precursors and (b) MMOs.

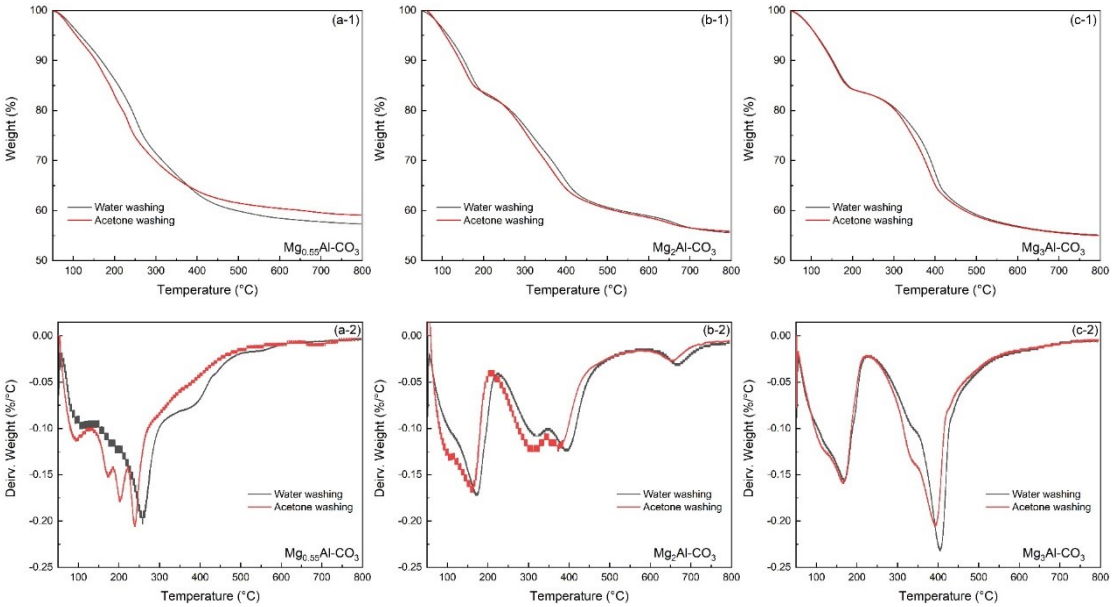

Figure S2. TGA and DTG analysis of (a) $Mg_{0.55}Al\text{-}CO_3$, (b) $Mg_2Al\text{-}CO_3$, and (c) $Mg_3Al\text{-}CO_3$ synthesized by co-precipitation with water washing and acetone washing.

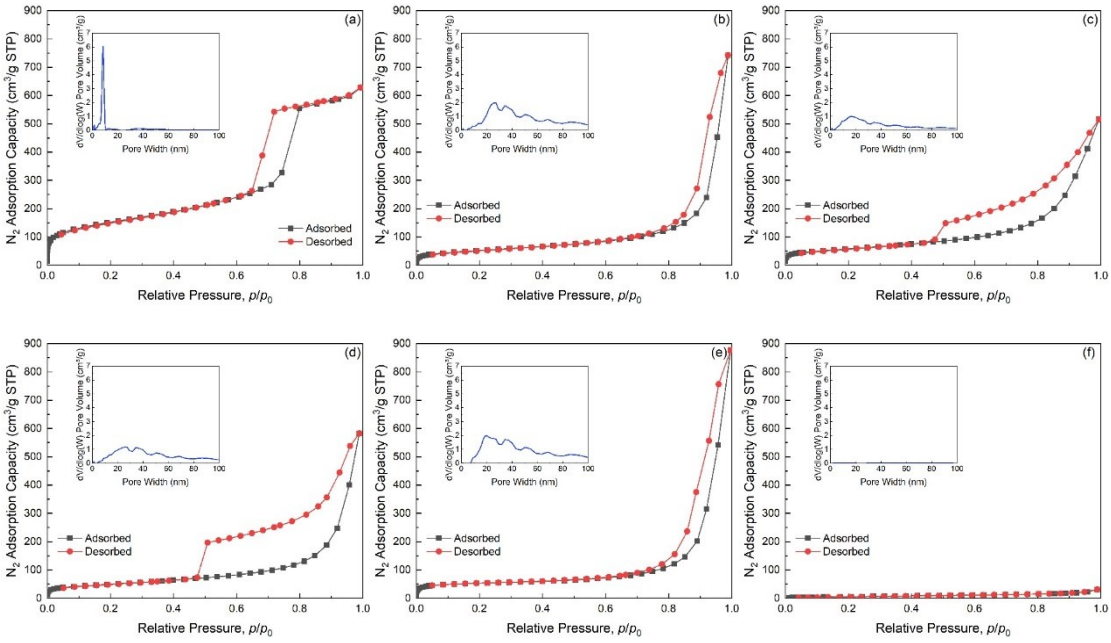

Figure S3. N_2 adsorption-desorption isotherms at 77 K and pore size distributions of (a) SBA-15, (b) $Mg_{0.55}Al$-O, (c) Mg_2Al-O, (d) Mg_3Al-O, (e) γ-Al_2O_3, (f) MgO.

Table S2. Textural properties of the supports.

Sample	S_{BET} ($m^2\ g^{-1}$)	D_p (nm)	V_p ($cm^3\ g^{-1}$)	V_{micro} ($cm^3\ g^{-1}$)
SBA-15	526	7.4	0.959	0.027
$Mg_{0.55}Al$-O	185	24.9	1.150	0.006
Mg_2Al-O	205	15.6	0.728	0
Mg_3Al-O	176	20.5	0.904	0.002
γ-Al_2O_3	172	31.6	1.172	0.023
MgO	23	8.3	0.047	0

S_{BET} Specific surface area ($m^2\ g^{-1}$)

D_p Average pore size (nm)

V_p Average pore volume ($cm^3\ g^{-1}$)

V_{micro} Average micropore volume ($cm^3\ g^{-1}$)

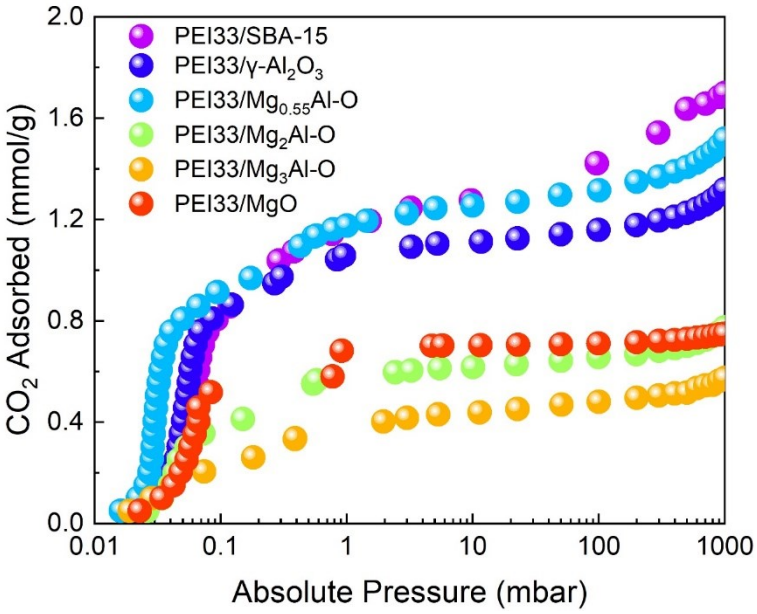

Figure S4. Characterization of CO_2 adsorption performance of poly(ethylenimine) (PEI)-based adsorbents in ultradilute conditions: screening of CO_2 adsorption isotherms at 25 °C for 33 wt.% PEI-impregnated supports.

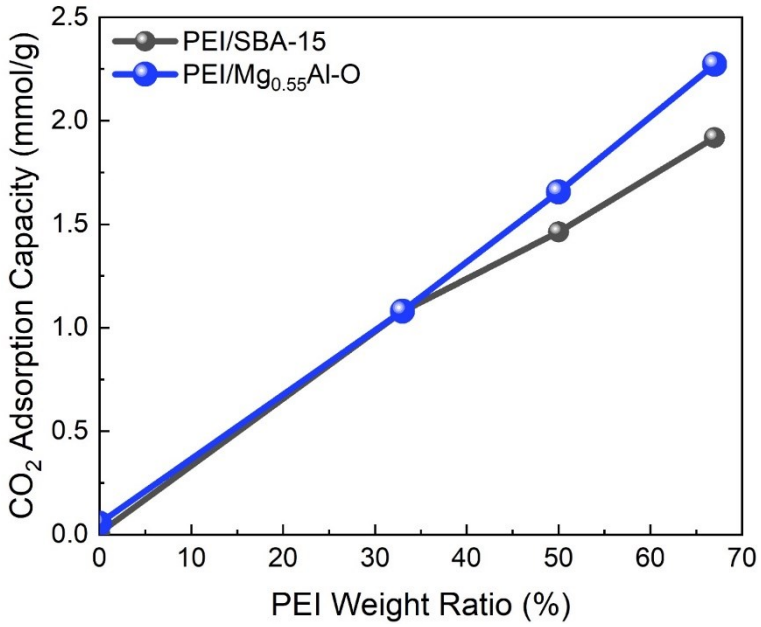

Figure S5. Characterization of CO_2 adsorption performance of poly(ethylenimine) (PEI)-based adsorbents in ultradilute conditions: effect of PEI weight ratios for PEI impregnated SBA-15 and $Mg_{0.55}Al$-O.

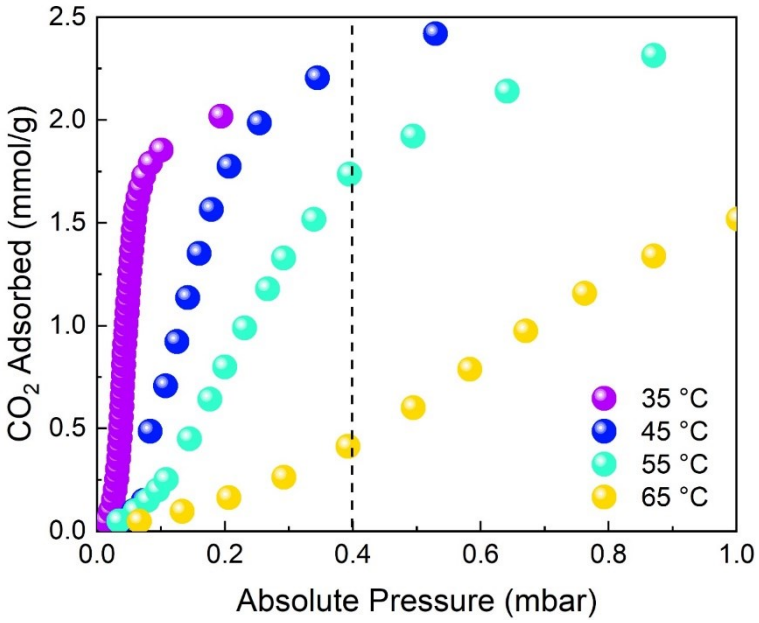

Figure S6. Characterization of CO_2 adsorption performance of poly(ethylenimine) (PEI)-based adsorbents in ultradilute conditions: CO_2 adsorption isotherms of PEI67/$Mg_{0.55}$Al-O at different adsorption temperatures.

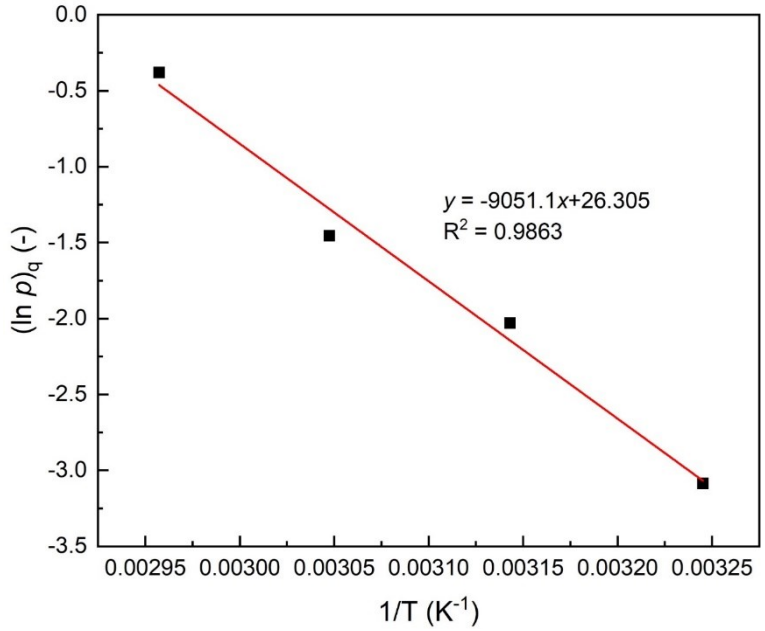

Figure S7. Fitting of CO_2 adsorption heat of PEI67/$Mg_{0.55}$Al-O at the CO_2 uptake of 1 mmol g^{-1}.

The isotherm data at 35, 45, 55, 65 °C was used to evaluate the adsorption of heat of PEI67/$Mg_{0.55}$Al-O. According to the Clausius−Clapeyron equation in Equation 1, The isosteric heat of adsorption, Q_{st}, can be determined by the slope of the fit line of $ln\, p$ versus $1/T$.

$$(ln\, p)_q = \left(\frac{Q_{st}}{R}\right)\left(\frac{1}{T}\right) + C \qquad (1)$$

p CO_2 pressure (mbar)

Q_{st} Adsorption of heat (J mol^{-1})

R Ideal gas constant (J mol^{-1} K^{-1})

T Temperature (K)

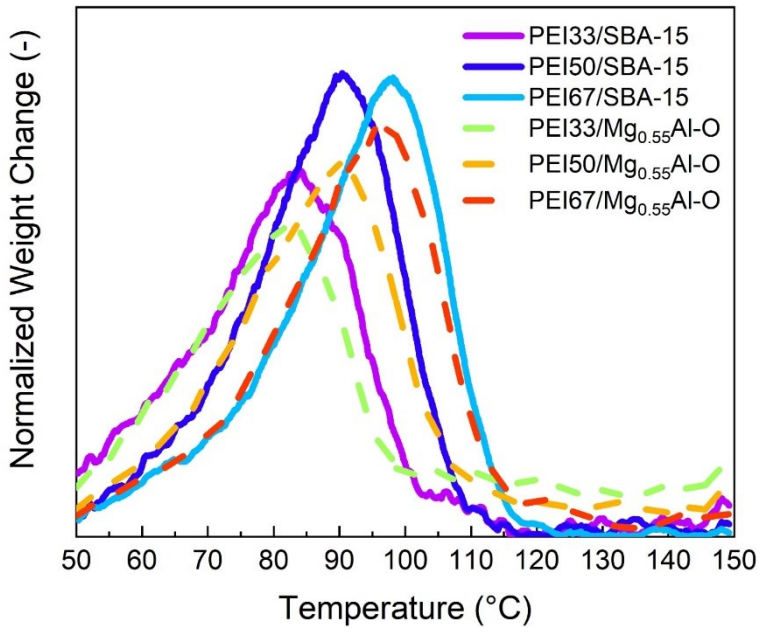

Figure S8. Characterization of CO_2 adsorption performance of poly(ethylenimine) (PEI)-based adsorbents in ultradilute conditions: temperature programmed desorption of PEI-impregnated SBA-15 and $Mg_{0.55}Al$-O.

Table S3. Textural properties of the PEI/supports.

Sample	S_{BET} ($m^2\ g^{-1}$)	D_p (nm)	V_p ($cm^3\ g^{-1}$)	V_{micro} ($cm^3\ g^{-1}$)
PEI33/$Mg_{0.55}$Al-O	110	27.0	0.642	0.010
PEI50/$Mg_{0.55}$Al-O	31	29.5	0.258	0.008
PEI67/$Mg_{0.55}$Al-O	20	4.4	0.020	0.002
PEI33/SBA-15	166	8.6	0.360	0.000
PEI50/SBA-15	17	8.1	0.033	0.000
PEI67/SBA-15	8	5.2	0.010	0.000

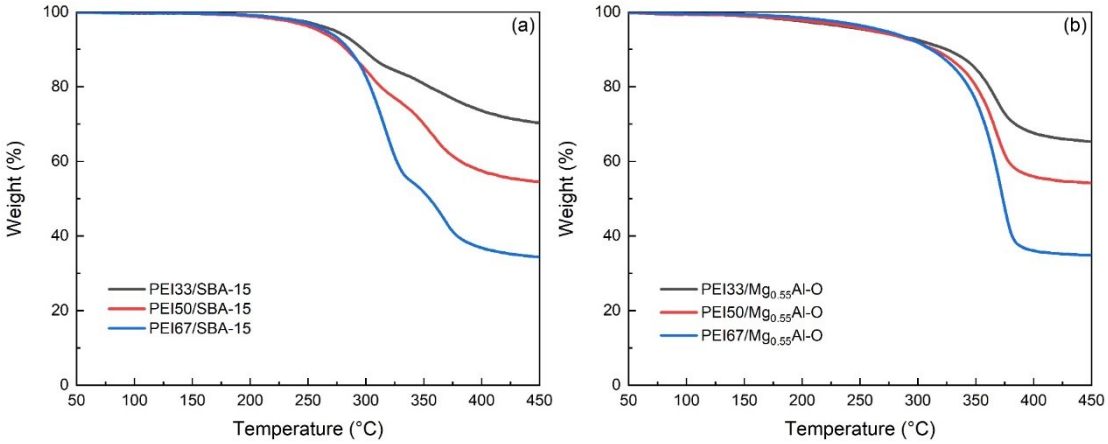

Figure S9. Thermal decomposition of PEI-based SBA-15 and $Mg_{0.55}Al$-O from 50 to 450 °C at a heating rate of 5 °C min^{-1} under N_2 flow.

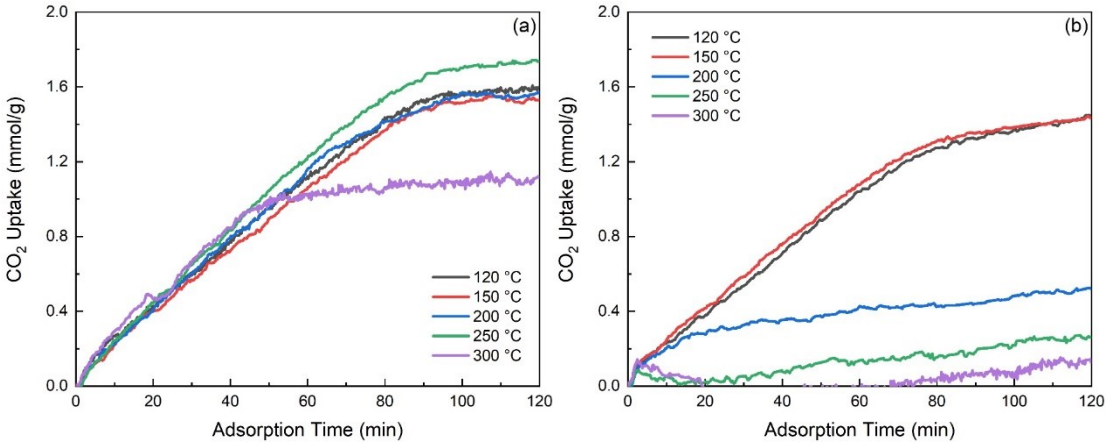

Figure S10. CO_2 uptake of (a) PEI67/$Mg_{0.55}$Al-O and (b) PEI67/SBA-15 at 400 ppm CO_2 and 25 °C after desorption at different temperatures.

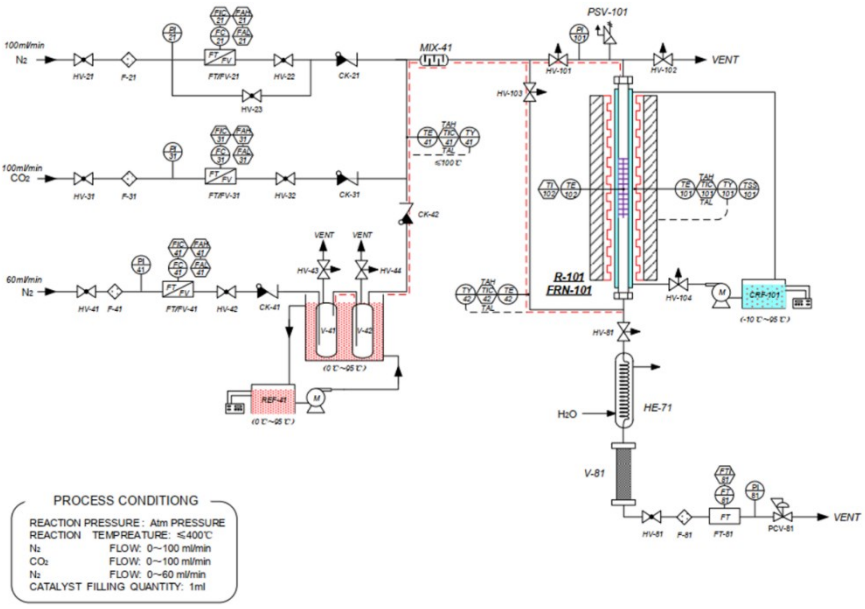

Figure S11. Experimental set-up of home-made fixed bed microreactor system.

The home-built fixed bed with a height of 120 mm and internal diameter of 6 mm was used to evaluate the cyclic stability of sample in the absence/presence of moisture. The flow rate of inlet gases (N_2, 400 ppm CO_2/N_2) was controlled by mass flow controllers (maximum flow rate: 120 mL min^{-1}) and the flow direction could be automatically switched via magnetic valves. The scrubbing bottle in a thermostatic water bath was used to generate 3–5% moisture for the inlet gases, where the water content before and after the fixed bed was monitored using temperature and humidity sensors. The fixed bed as a stainless-steel tube was sequenced filled with silica sand, silica wool, samples (0.8 g), silica wool, and silica sand to insure all the samples was within the flat-temperature zone. The CO_2 concentration in the outlet gas after passing through a $CaCl_2$ drying tube was continuously detected by an THA100S non-dispersive infrared analyzer (0−600 ppm, ±2% full scale).

During the cyclic operation, the fixed bed was first heated by a temperature control stove to 120 °C followed by a counter-current N_2 purge with a flow rate of 100 mL min^{-1} for 60 min. The circulating oil bath was then opened to rapidly cool down the fixed bed to 25 °C. In the adsorption step, 400 ppm CO_2 in N_2 with a flow rate of 100 mL min^{-1} was co-currently added into the fixed bed for 120 min. The CO_2 adsorption capacity in the stability tests was calculated according to equation 2.

$$q = \frac{\int_0^t \left(C_{CO_2,in} - C_{CO_2,out}\right) Q_{in} dt}{m_{sample}} \quad (2)$$

q CO_2 adsorption capacity (mol kg^{-1})

$C_{CO_2,in}$ Inlet gas CO_2 concentration (mol m^{-3})

$C_{CO_2,out}$ Outlet gas CO_2 concentration (mol m^{-3})

Q_{in} Inlet gas flow rate (m^3 s^{-1})

m_{sample} Sample initial mass (kg)

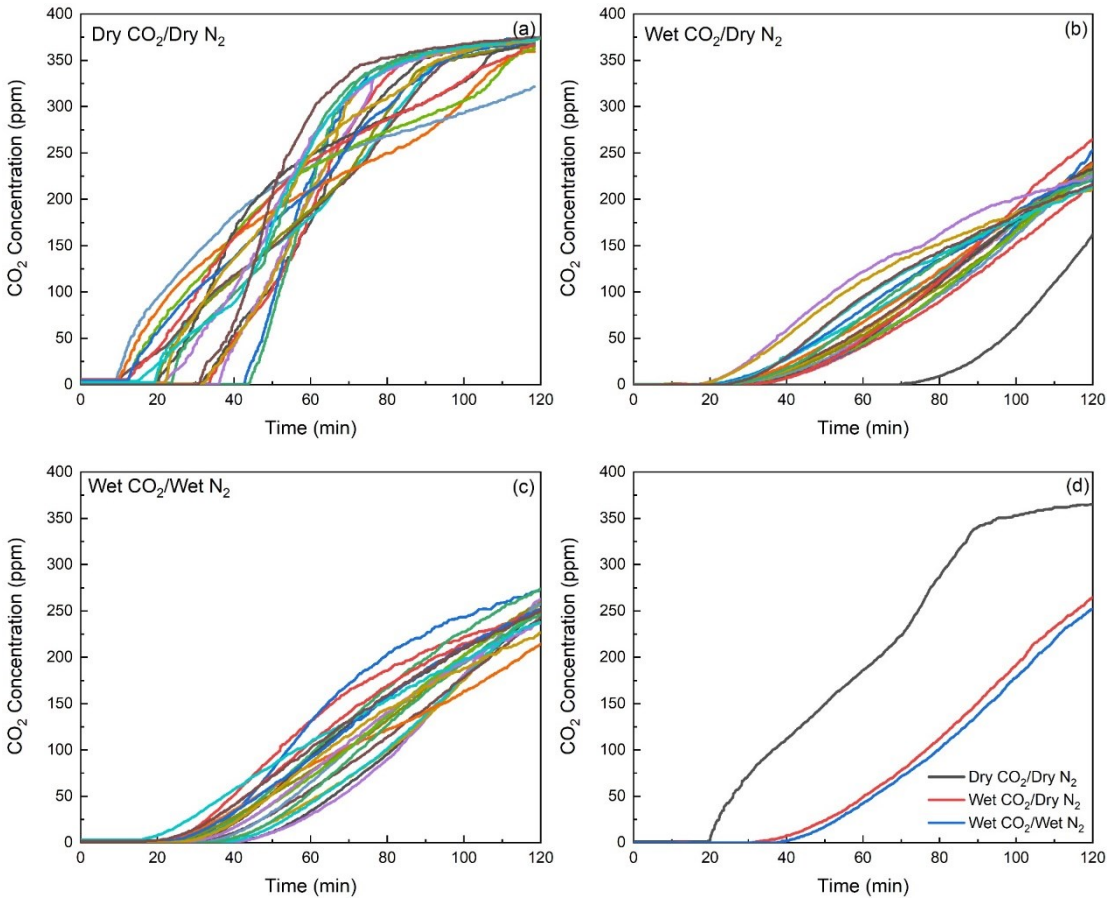

Figure S12. CO_2 breakthrough curves of PEI67/$Mg_{0.55}$Al-O during multi cycles (a) for adsorption in dry CO_2 and desorption in dry N_2, (b) for adsorption in wet CO_2 and desorption in dry N_2, (c) for adsorption in wet CO_2 and desorption in wet N_2, and (d) after reaching steady state.